[CANCER RESEARCH 64, 6495–6502, September 15, 2004]

In vivo Detection of Gastric Cancer in Rats by Electron Paramagnetic Resonance Imaging

Tomiko Mikuni,[1,2,3,4] Guanglong He,[1,2] Sergey Petryakov,[1,2] Mohanad M. Fallouh,[1,2] Yuanmu Deng,[1,2] Ryu Ishihara,[3] Periannan Kuppusamy,[1,2] Masaharu Tatsuta,[3] and Jay L. Zweier[1,2]

[1]Center for Biomedical Electron Paramagnetic Resonance Spectroscopy and Imaging, Davis Heart and Lung Research Institute and [2]Division of Cardiovascular Medicine, Department of Internal Medicine, The Ohio State University College of Medicine, Columbus, Ohio; and Departments of [3]Gastrointestinal Oncology and [4]Clinical Laboratory, Osaka Medical Center for Cancer and Cardiovascular Diseases, Osaka, Japan

ABSTRACT

Electron paramagnetic resonance imaging (EPRI) enables noninvasive spatial mapping of free radical metabolism and has recently been shown to provide *in vivo* physiologic information regarding alterations in the redox state of tumors and neoplastic tissues. With the use of nitroxide spin probes, it has been shown that certain tumors possess a highly reduced state. To determine whether EPRI can be used for early detection and visualization of gastric carcinoma based on its altered redox metabolism, studies were performed in a rat gastric cancer model induced by 1-methyl-3-nitro-1-nitrosoguanidine. Using a specialized 750 MHz resonator and EPRI instrument, a technique was developed for imaging nitroxide radicals in the whole stomach. *In vivo* three-dimensional EPRI of the stomach of rats with continuous intravenous administration of nitroxide 3-carboxamido-2,2,5,5-tetramethylpyrrolidine-*N*-oxyl (3-carbamoyl-proxyl) [3-CP] was performed. Whereas electron paramagnetic resonance images from untreated controls provide a uniform visualization of the stomach mucosa and wall, in the treated rats with gastric cancer, holes were present in the image at the locations of tumors. With localized spectroscopy, it was confirmed that the tumor regions were devoid of signal, and this was largely due to the presence of a more reduced state with rapid reduction of nitroxide. Pharmacokinetic studies indicated that 3-CP in tumors was rapidly reduced to an undetectable level, whereas the 3-CP levels in normal stomach tissue persisted. Near-infrared reflectance measurements of indocyanine green dye uptake indicated that there were no significant differences in tumor *versus* normal mucosal perfusion. From these results, we concluded that gastric cancer tumors could be distinguished from normal tissue based primarily on the marked difference in their rate of radical metabolism. Because alterations in cellular redox state and radical metabolism are of critical importance in tumor biology and treatment, this methodology should provide an important new tool for the study and visualization of gastric carcinoma and may also be of use in other cancer models.

INTRODUCTION

Gastric cancer is the second leading cause of cancer death in Japan and the Far East (1) and is also a less common but notable cause of cancer mortality in the United States and Europe (2). Despite major research and clinical efforts, the number of deaths from gastric cancer has not decreased in recent years, and the major clinical goal has been early detection and surgical excision. There have also been major efforts to better understand the mechanisms responsible for oncogenesis in the stomach, with an eye toward possible prevention. A number of animal models of stomach cancer have been developed (3–5). Among these, the 1-methyl-3-nitro-1-nitrosoguanidine (MNNG) model has proven to be very useful, enabling the study of mechanisms and pathogenesis of gastric carcinoma in rats (6). It has been shown that MNNG administration results in increased oxygen radical generation in the mucosa of the stomach, and this oxidative injury is thought to be a key step in oncogenesis (7).

There is evidence that oxygen radical generation and altered tissue redox state are key factors in the process of tumor promotion and transformation (7, 8). In recent years, it has also become increasingly clear that oxygen radicals have a key role as second messengers in regulating the process of cellular growth and cell death (9). Recently, it has been reported that a number of cancer-linked genes are associated with alterations in cellular redox state and free radical generation (10). It is also clear that a number of modalities of cancer treatment are based on induction of high levels of oxygen radical formation that lead to tumor necrosis or apoptosis. Classical radiation therapy induces oxygen-dependent formation of hydroxyl radical, leading to cell death. A number of chemotherapeutic agents, including Adriamycin and bleomycin, trigger oxygen radical formation that is involved in their mechanisms of tumor killing (11, 12). Therefore, there has been a great need for techniques to accurately assess cellular redox state and altered radical generation in the process of oncogenesis, tumor biology, and tumor treatment.

In vivo electron paramagnetic resonance imaging (EPRI) methods have been developed to enable noninvasive determination of the spatial distribution of free radicals and of alterations in free radical metabolism associated with disease (13–15). EPRI is a powerful technique able to measure free radical metabolism and redox state and can provide high sensitivity, specificity and spatial resolution. It has been extensively used to noninvasively measure the distribution and kinetics of transient/stable free radicals in biological tissues (15–18). The electron paramagnetic resonance (EPR) spectrum is a fingerprint of free radicals with their unique hyperfine structures. This technique is extremely sensitive, and it can detect free radicals in concentrations as low as 10 nmol/L with an *in vivo* imaging sensitivity that extends down to μmol/L levels (19, 20).

Furthermore, in recent years, this technique, along with appropriate nitroxide spin probes, has been extensively applied to provide information about the redox state within organs of living animals and alterations associated with disease (17, 21). These techniques have been applied to measure and map the distribution and metabolism of free radicals in a number of organs and tissues including the heart, brain, gastrointestinal tract, and, most recently, in tumors (16, 21–23). These paramagnetic nitroxide probes are bioreduced to the corresponding EPR silent hydroxylamines by mitochondrial reduction and intercellular antioxidants, and this reduction is markedly enhanced under hypoxic conditions (24–26). Hypoxic tissues can be readily distinguished from normoxic tissues based on the rate of nitroxide reduction. Many solid tumors contain hypoxic regions (27–29), and it has been shown previously (21) that the low pO_2 in implanted tumors compared with that in normal tissue results in a more rapid reduction of the nitroxides, and this process has been measured previously and mapped in *in vivo* fibrosarcomas in mice by EPR spectroscopy and imaging.

Therefore, the present study was performed in an effort to determine whether EPR spectroscopy and imaging techniques can be

Received 2/9/04; revised 6/28/04; accepted 7/9/04.

The costs of publication of this article were defrayed in part by the payment of page charges. This article must therefore be hereby marked *advertisement* in accordance with 18 U.S.C. Section 1734 solely to indicate this fact.

Note: T. Mikuni and G. He contributed equally to this work.

Requests for reprints: Jay L. Zweier, 110G Davis Heart and Lung Research Institute, 473 West 12th Avenue, Columbus, OH 43210-1252. E-mail: zweier-1@medctr.osu.edu.

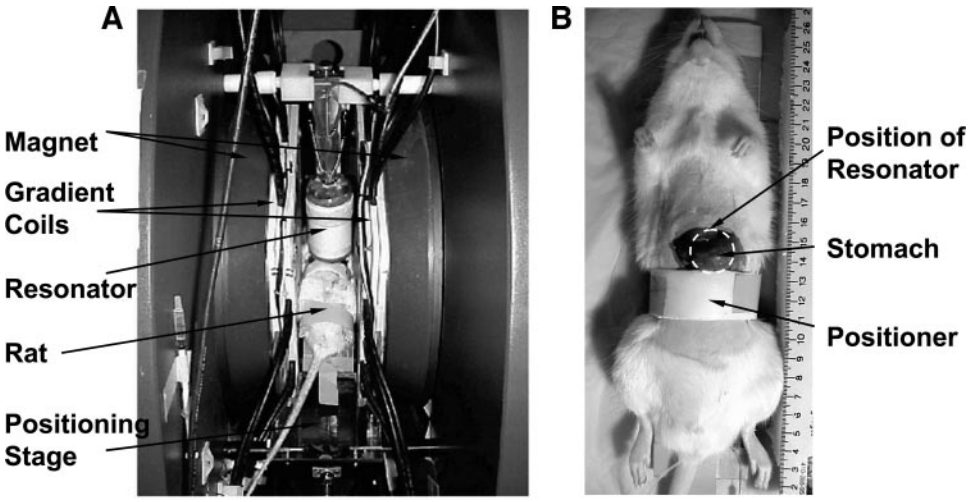

Fig. 1. Photograph of EPRI instrumentation and rat preparation for EPRI measurement of the stomach. In *A*, the components of EPRI instrument are labeled. In *B*, rat preparation is seen after laparotomy, with the externalized stomach held in an uplifted position by the holder, which can be seen as the *white plastic piece* just below the stomach. The *dashed white circle* shows the position where the resonator was centered.

applied to provide identification of gastric tumors with differentiation from surrounding tissue as well as information regarding alterations in cellular redox state associated with these neoplastic cells. Experiments were performed in a MNNG-induced model of gastric carcinoma with EPRI and localized EPR spectroscopy to measure and map the distribution and metabolism of a nitroxide radical redox probe. We observe that gastric tumors exhibit a distinctly different radical distribution and redox state than normal stomach tissue, and this enables their detection and spatial localization by EPRI techniques.

MATERIALS AND METHODS

Chemicals. The gastric carcinogen MNNG and nitroxide free radical 3-carboxamido-2,2,5,5-tetramethylpyrrolidine-*N*-oxyl (3-carbamoyl-proxyl) [3-CP] were purchased from Aldrich Chemical Co. (Milwaukee, WI). Sodium pentobarbital was from Abbott Laboratories (Chicago, IL), and triarylmethyl radical for EPRI of phantom was provided by Nycomed Innovations (Ox063, Malmo, Sweden). Indocyanine green (ICG) for near-infrared reflectance (NIR) imaging was from Daiichi Pharmaceutical Co. Ltd. (Tokyo, Japan). All other reagents were purchased from Sigma (St. Louis, MO).

Induction of Gastric Carcinoma in Rats. Six-week-old Wistar rats were purchased from Japan SLC (Hamamatsu, Shizuoka, Japan) and housed in suspended wire-bottomed metal cages in animal quarters maintained at a temperature of 21°C to 22°C and a humidity of 30% to 50% with a 12-hour light/dark cycle. Starting at 3 weeks of age, rats were given drinking water containing MNNG at a concentration of 50 μg/mL for 25 weeks. The MNNG solution was supplied from bottles covered with aluminum foil to prevent photolysis and refilled every other day as reported previously (30). After 25 weeks, MNNG administration was stopped, and normal tap water was supplied. Rats had free access to regular chow pellets (Nihon-Norsan, Yokohama, Japan). At 65 to 69 weeks, animals were used for EPRI and EPR spectroscopy experiments. Normal rats given normal tap water instead of MNNG solution served as tumor-free controls. Eight rats with gastric cancer tumors of 2 to 8 mm in diameter and six normal rats were used. The tumors could be readily identified by external palpation of the firm nodules in the stomach, and this was subsequently visually confirmed when the stomach was incised, with further verification by histology.

Electron Paramagnetic Resonance Imaging Measurements. Three-dimensional EPRI measurements were performed in a manner similar to that described previously (31, 32), with only slight modifications using EPRI instrumentation built at The Ohio State University, Center for Biomedical EPRI, consisting of a 750 MHz EPR spectrometer, three sets of water-cooled gradient coils attached to the magnet pole pieces, and a specially designed bridged loop-gap surface resonator customized for gastric imaging. This resonator has two-bridged gaps, a loop diameter of 25 mm with a length of 28 mm, and is surrounded by a cylindrical shield of 50 mm in diameter (Fig. 1*A*). A detailed description of this resonator design is to be reported separately.[5] The EPRI parameters were as follows: frequency, 750 MHz; microwave power, 50 mW; modulation amplitude, 1 G; scan width, 25.6 G, scan time, 5 seconds; time constant, 40 milliseconds; gradient field, 8 G/cm. The sensitive imaging region provided by the resonator was mapped with three-dimensional EPRI measurements of a cylindrical phantom filled with the sharp single-line triarylmethyl radical. From this image, a map of H_1 field magnitude was obtained and used to correct for any H_1 inhomogeneity in the image space. EPRI of the phantom showed that the radical distribution could be measured within a diameter of 29 mm in the plane of the resonator surface and to a depth of 20 mm, adequate to image the uplifted stomach. Image data are displayed as either three-dimensional surface-rendered images or as a series of two-dimensional slices continuously cut with 0.25 mm thickness along the *ZX* plane.

Animal Preparation. Before the measurements, rats were fasted for 12 h except for water *ad libitum*. Rats were anesthetized with intraperitoneal injection of 50 mg/kg sodium pentobarbital. The tail vein was cannulated with a heparin-filled catheter for infusion of nitroxide solution. After this, the hair on the abdomen was shaved, the rat was placed on a hard plastic holder, and the abdomen was opened with a small incision. The stomach was lifted up from the peritoneal cavity and maintained in this uplifted position with a plastic holder with retracting tab adjacent to posterior aspect of the lesser curvature of the stomach (Fig. 1*B*). The rat with the holder was then placed on the positioning stage of EPRI instrument (Fig. 1*A*), and then the resonator was lowered until the stomach was optimally placed within or adjacent to the resonator surface and fixed in place. EPRI measurements of the stomach were performed immediately after administration of a 2-minute intravenous load of 1.5 mL of 300 mmol/L 3-CP. A continuous intravenous infusion of 300 mmol/L 3-CP was then continued at a rate of 0.035 mL/min. This maintenance dose provided a near constant EPR signal within the stomach for the duration of the imaging experiments. To provide verification that the immobilization process/positioner does not alter perfusion to the normal and tumor regions of the stomach, laser Doppler flow measurements were performed using a floLAB laser Doppler blood flow monitor (Moor Instruments Limited, Devon, United Kingdom) with a MP2 probe of 30 mm in length and 6 mm in diameter. No alterations in flow were seen with the immobilization process for exteriorization and EPRI.

Localized Electron Paramagnetic Resonance Spectroscopy Measurements. Localized EPR spectroscopy measurements of the distribution of 3-CP in tumors and normal gastric tissue were performed using a surface coil resonator with a diameter of 10 mm and a sensitive depth of 7 mm, and an L-band microwave bridge. EPR variables were as follows: microwave power,

[5] S. Petryakov, G. He, P. Kuppusamy, J. L. Zweier. Bridged loop-gap resonator design for topical electron paramagnetic resonance imaging at 750 MHz, manuscript in preparation.

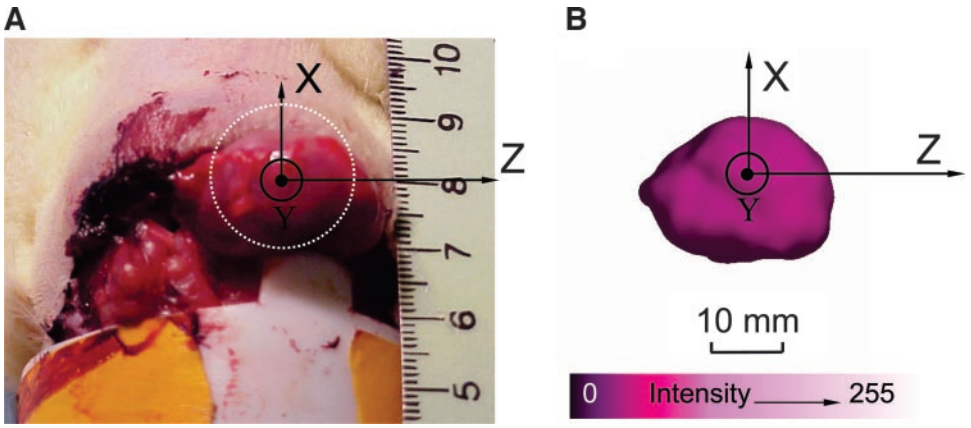

Fig. 2. EPRI of free radical distribution in normal stomach of a living rat after loading and continuous intravenous infusion of 3-CP nitroxide label. *A*, photo of the animal preparation used with externalized, uplifted stomach. *B*, surface-rendered three-dimensional free radical image of the stomach. This photograph is shown with the same scale and orientation to enable comparison of the free radical image of the stomach with the visual image of the stomach preparation. The center of the resonator was placed over the stomach against the greater curvature. The long axis of the body was along the *X* axis, and the lateral transverse direction was along the *Z* axis, whereas the *Y* axis extends transverse to the *XZ* plane in a posterior to anterior direction.

32 mW; modulation amplitude, 1 G; scan width, 60 G; scan time, 15 seconds; and time constant, 80 milliseconds.

***In vivo* Indocyanine Green–Near-Infrared Reflectance Imaging of Perfusion.** Gurfinkel *et al.* (33) showed that ICG acts as a blood pool or blood persistence agent without selective uptake or efflux mechanism by *in vivo* NIR images of the phamacokinetic delivery of ICG. Because the rates of capillary permeability and blood pool or blood persistence are determined by blood flow, using NIR imaging with ICG, the differences in blood flow were examined by comparison of the rates of ICG distribution in tumor and normal tissue. Next, with ICG-NIR images, we examined whether blood was delivered in equivalent amounts to normal mucosa *versus* tumor regions. Furthermore, we examined whether the results might be affected by cutting the stomach. That is, the stomach was exteriorized and opened along the greater curvature, according to the methods described in the EPRI experiment and where there are few blood vessels. The opened stomach was then maintained, mucosa up, in a lifted position by a plastic holder. After intravenous administration of 5.0 mg/kg ICG to rats, a 25-mW tungsten halogen light fitted with an 805 nm band pass interference filter illuminated the surface of the mucosa tissue. With the video camera, recording of the ICG-NIR of the mucosa surface generated from within the tissue volume as great as 2 mm was started on a nonintensified videotape 2 minutes after injection of ICG. The frame, on which the first maximal ICG-NIR was recorded, was studied for the two-dimensional image of the ICG uptake rate. Numerical analysis of the pseudo-color images was performed according to the manufacturer's specifications (Olympus Optical Co., Ltd., Tokyo, Japan).

Histology. After the experiments, each stomach was sectioned for routine histologic examination. The stomach was opened along the greater curvature, pinned flat on a mat, fixed with 10% formalin (pH 7.4), and stained with hematoxylin and eosin. Adenocarcinomas were defined as neoplastic tumors with involvement of the submucosa or deeper layers such as the muscle layer and serosa (34).

RESULTS

Electron Paramagnetic Resonance Imaging of the Stomach. The three-dimensional EPRI of the normal stomach of untreated animals exhibited a homogenous distribution of nitroxide spin label without any regions of voids or holes of lower radical concentration (Fig. 2). The EPR image appeared similar to that of the visual image of the stomach. In contrast, three-dimensional EPRI of the treated animals with palpable gastric tumors exhibited prominent holes at locations corresponding to the gastric cancer tumors (Fig. 3). As illustrated in Fig. 3*C*, the stomach was incised just above the greater curvature after EPRI measurement. The mucosal surface was exposed, revealing a tumor of about 8 mm (Fig. 3*D*, *dotted circle*) present in the antrum. As shown in the diagram, the tumor was present along the greater curvature in the antrum and curved along the *XY* plane inward toward the abdomen. The three-dimensional EPR image of the tumor-

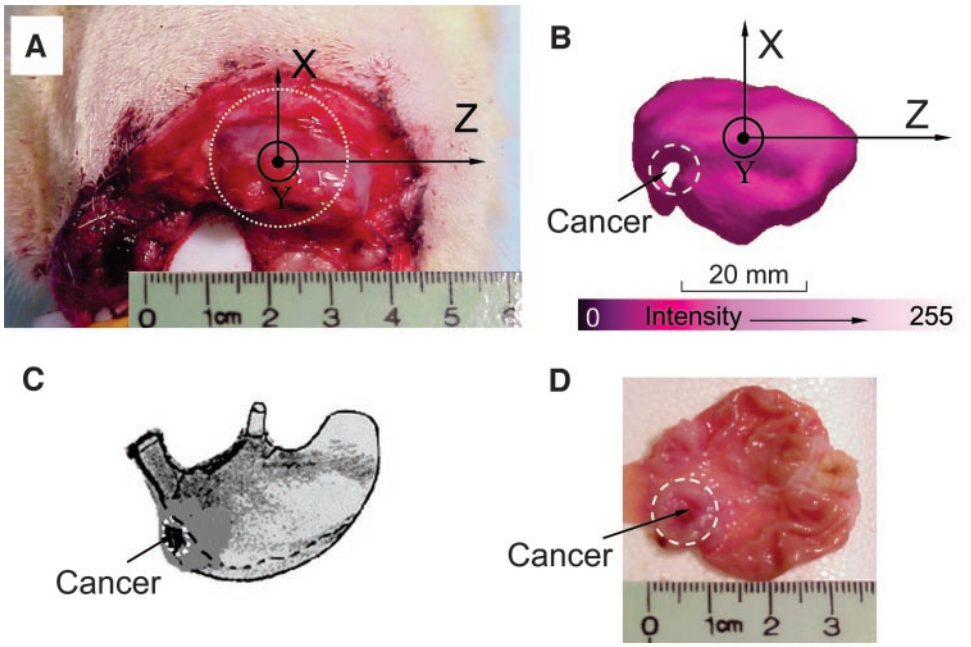

Fig. 3. EPRI of free radical distribution in the stomach of a living rat with gastric cancer obtained after loading and continuous intravenous infusion of 3-CP nitroxide label. *A* shows a photo of animal preparation with externalized uplifted stomach; the *dashed circle* shows the location of the resonator. *B* shows the surface-rendered three-dimensional free radical image of the tumor-containing stomach; the *dashed circle* shows the location of the tumor determined by palpation and confirmed by open examination after excision. The orientations of *A* and *B* are as described in Fig. 1. *C*, a sketch of the stomach; the *dashed line* shows the incision line along the greater curvature. *D* shows the mucosal surface of the opened stomach; the location of the 8-mm tumor is shown within the *dashed white circle*.

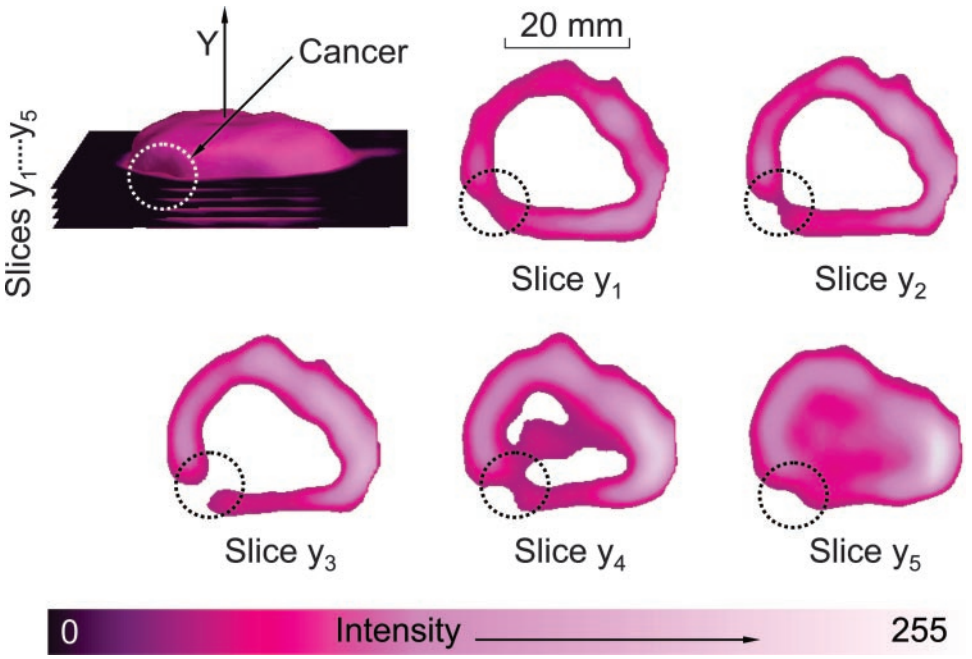

Fig. 4. Two-dimensional slices of the three-dimensional EPR image data of the tumor-containing stomach. The slices are cuts of the three-dimensional image orthogonal to the *Y* axis. The absence of free radical signal at the site of the tumor is clearly seen in these two-dimensional slices. The absence of signal extends from the mucosal surface through the wall of the stomach. The *black dotted circle* indicates the position of the tumor.

bearing stomach in Fig. 3*B* exhibited a prominent hole measuring about 6 mm in diameter at the location in the antrum on the greater curvature of the stomach. At this location, a hole devoid of nitroxide radical signal was seen, which was surrounded by an annular ring of low signal intensity, whereas the image of the surrounding stomach was otherwise homogeneous. The location of this hole in the EPR image corresponded to the location of the palpated tumor labeled in Fig. 3*C* that was visualized after subsequent incision and exposure of the luminal surface. To better visualize the tumor, a series of two-dimensional slices are shown from the three-dimensional image data. These images were corrected to compensate for resonator H_1 inhomogeneity as described previously (35). These image cuts along the *Y* axis clearly depict the relative absence of signal intensity at the location of the tumor (Fig. 4). Thus, EPRI was able to distinguish and map the location of gastric cancer tumor based on the relative absence of nitroxide signal within the tumor.

Localized Electron Paramagnetic Resonance Spectroscopy Measurements of the Normal Stomach and Tumor. To further confirm the relative differences in nitroxide signal intensity in the normal gastric wall *versus* the tumor, experiments were performed in a number of animals, measuring the localized signal of the stomach with a 10-mm-diameter surface coil placed directly against the normal gastric wall or directly centered at the location of the palpated tumor. Measurements were performed on the stomachs of a series of control and tumor-bearing animals after intravenous bolus infusion of 1.5 mL of 300 mmol/L 3-CP over 2 minutes. EPR spectra were recorded, and EPR signal intensity was measured as a function of time. In general, a trend was seen that the larger the tumor, the lower the observed signal.

In Fig. 5, measurements of the observed signal intensity are shown from the stomachs of three animals. The first contained a large tumor with a diameter of 8 mm that was almost large enough to fill the sensitive volume of the surface coil. The second contained three small adjacent tumors, each of only 2 mm in diameter, that only filled a small portion of the sensitive volume, and the third was of a similar antral region of a control non-tumor-containing stomach. The first point in this graph shows the signal intensity seen immediately after the 3-CP bolus infusion. In the stomach with the large tumor, a much lower signal magnitude was seen, whereas in the presence of smaller tumors, only a modest decrease was seen. In general, it was observed that the decrease in signal paralleled the portion of the sensitive volume of the resonator filled with tumor rather than normal tissue.

We examined the time dependence of the signal decay in each stomach, and it was observed that in contrast to the lower signal levels detected in the presence of tumor, the kinetic decay of the observed nitroxide signal was similar in the tumor-containing stomach and normal stomach. In each case, a half-life in the range of 9.1 ± 0.9 minutes was observed with values of 10.0, 8.6, and 8.2 minutes for the signal decay seen in *A*, *B*, and *C*, respectively (Fig. 5). Because the ratio of tumor volume to normal tissue within the resonator paralleled the observed decrease in signal and the decay kinetics were identical to that in normal tissue, this suggested that the observed signals in the

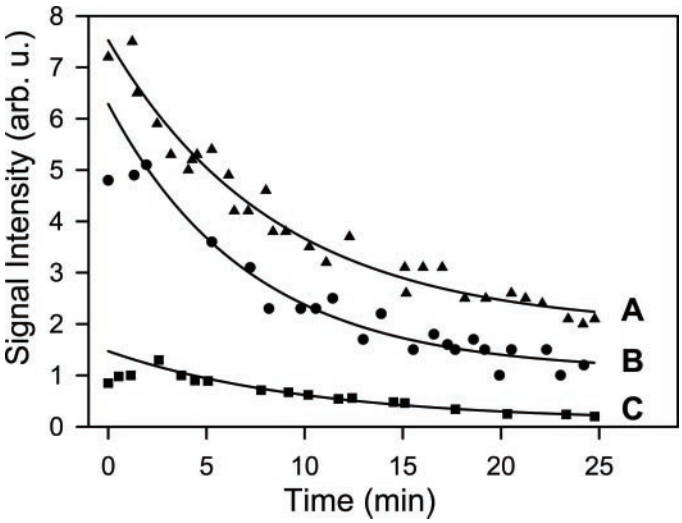

Fig. 5. EPR spectroscopy measurements of the pharmacokinetics of the 3-CP nitroxide label in localized regions of the stomach of control or tumor-bearing rats. Localized EPR spectra were recorded from the antral regions of a control stomach (*A*), a stomach with two small adjacent tumors of 2 mm in diameter (*B*), and a stomach with a large tumor of 8-mm in diameter (*C*). Measurements were performed at 1.2 GHz using a small surface coil resonator. The surface coil placement over the tumors was based on palpation of the firm tumor mass and confirmed by subsequent incision with open visualization followed by histology.

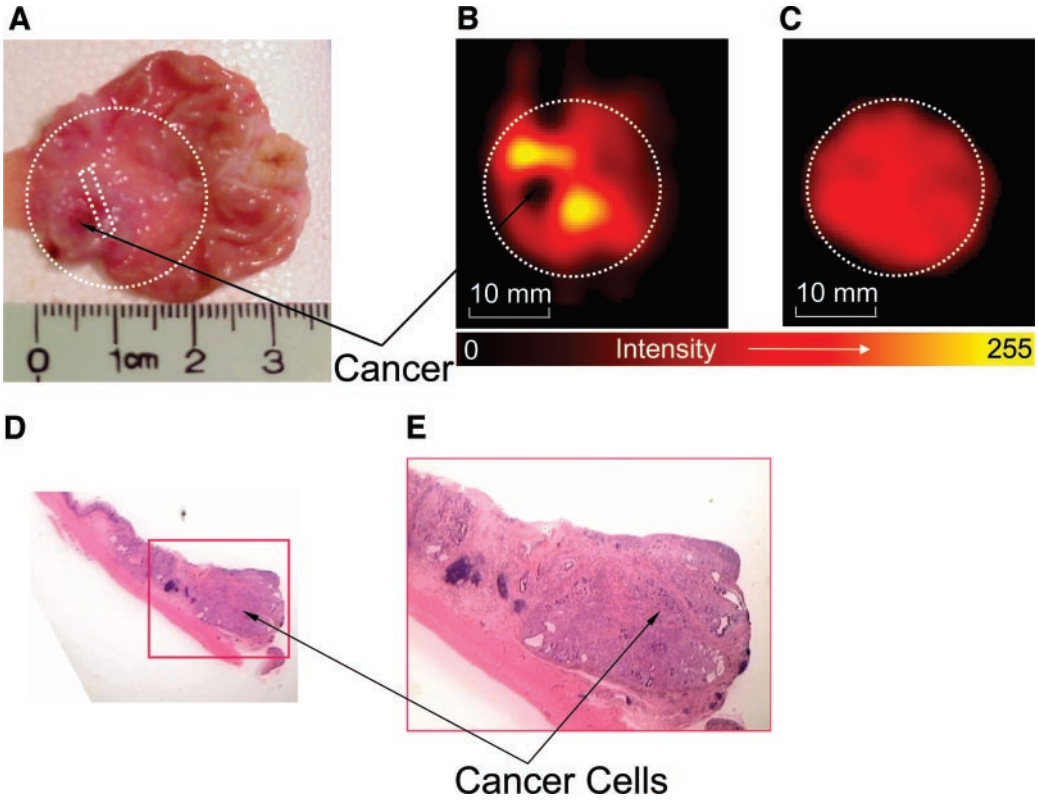

Fig. 6. *A*, photo of incised open stomach, and *B*, EPR image data of the free radical distribution of the 3-CP nitroxide label directly applied to the surface of the gastric mucosa of the incised stomach. The stomach was rapidly excised and opened to expose the mucosal surface, and then 10 mmol/L nitroxide solution was topically applied to the mucosal surface. The resonator was centered over this area, and two-dimensional spatial imaging was performed. The two-dimensional EPR image data obtained showed a clear void at the site of the cancer, suggesting much faster reduction of the nitroxide in the tumor than in the surrounding tissue. *C* shows the restored image after applying 20 mmol/L ferricyanide solution topically to the opened stomach. *D* and *E* show the histology of the tumor-containing stomach. A section through the antrum at the location of the tumor was taken, as shown in the *dashed white lines* in the image of opened stomach in *A*. In *D*, the hematoxylin and eosin-stained section is shown at low magnification. In *E*, the tumor is shown at higher magnification to enable visualization of the cancer cells. The images shown are from the stomach that underwent *in vivo* imaging in Figs. 3 and 4.

tumor-containing stomachs were derived almost entirely from the normal gastric tissue surrounding the tumor. Thus, it appears that the observed signal arises almost entirely from normal stomach tissue and is absent from the tumor. This confirms the EPRI observations of a hole with an apparent lack of nitroxide signal at the tumor sites within the stomach and suggests that either the tumor tissue exists in a highly reduced state or there is less uptake of 3-CP within the tumor.

In an effort to determine whether the relative absence of signal in the tumor was due to the presence of a highly reduced state and not simply to lack of nitroxide uptake in the tumor, studies were performed in an incised stomach preparation with topical application of the 3-CP nitroxide solution. The stomach was rapidly removed from the rat, opened along the greater curvature, and fixed on a sample holder plate with the mucosal surface oriented upward. Similar to the results seen in the intact closed stomach, after topical application of the nitroxide, a void in the image was seen at the location of the tumor, indicating a much more rapid rate of reduction than in the surrounding normal tissue (Fig. 6). With topical application of the oxidizing agent ferricyanide (20 mmol/L), which converts the reduced EPR-silent hydroxylamine back to EPR-detectable nitroxide, the lower signal level in the tumor was reversed, as shown in Fig. 6*C*.

Thus, the gastric tumor tissue appears to intrinsically exhibit a much more rapid rate of nitroxide reduction, and this gives rise to the hole observed in the EPR image.

Histology of Gastric Cancer. Histologic studies indicated that all of the tumors occurred in the antral mucosa and that gastric tumors were all histologically well differentiated adenocarcinomas. The sample corresponding to the tumor-containing stomach whose EPRI data are presented in Figs. 3 and 4 is shown in Fig. 6. Within the tumor, central islands of necrosis and surrounding fibrosis were seen (Fig. 6*E*, *arrow*).

***In vivo* Indocyanine Green—Near-Infrared Images of Perfusion in Normal Stomach and Tumor.** In an effort to determine whether the relative absence of signal in the tumor was due to the presence of a highly reduced state and not simply a lack of perfusion and compound uptake in the tumor, studies were performed using *in vivo* ICG-NIR imaging of tumor-bearing stomach. We examined whether the immobilization process that was required for exteriorization of the stomach altered perfusion to the normal tissue and tumor; furthermore, we examined whether the agent was delivered in equivalent amounts to normal mucosa and tumor. The stomach was pulled out from the abdomen, opened, and put on the holder under anesthesia as shown in Fig. 7*A*, and video recording of the ICG-NIR signal within the tissue was started 2 minutes after intravenous administration of ICG. Fig. 7*B* shows the image of ICG uptake rates at the first maximum uptake. The rate of ICG uptake in the tumor (the *white solid circle*, except for halation spots) was determined as 85% of the rate in the normal tissue (the *white dotted circle*). The pseudo-color image of the rate of ICG uptake in Fig. 7*C* also exhibited no significant difference in the color between the tumor (*white solid circle*) and the surrounding normal tissue. From these results, we confirmed that there was no significant difference in ICG uptake rate between tumor and normal tissue after the stomach was immobilized on the holder, and we also confirmed that ICG was delivered in equivalent amounts to normal and tumor regions after intravenous administration. Furthermore, it was confirmed that there was no significant difference in

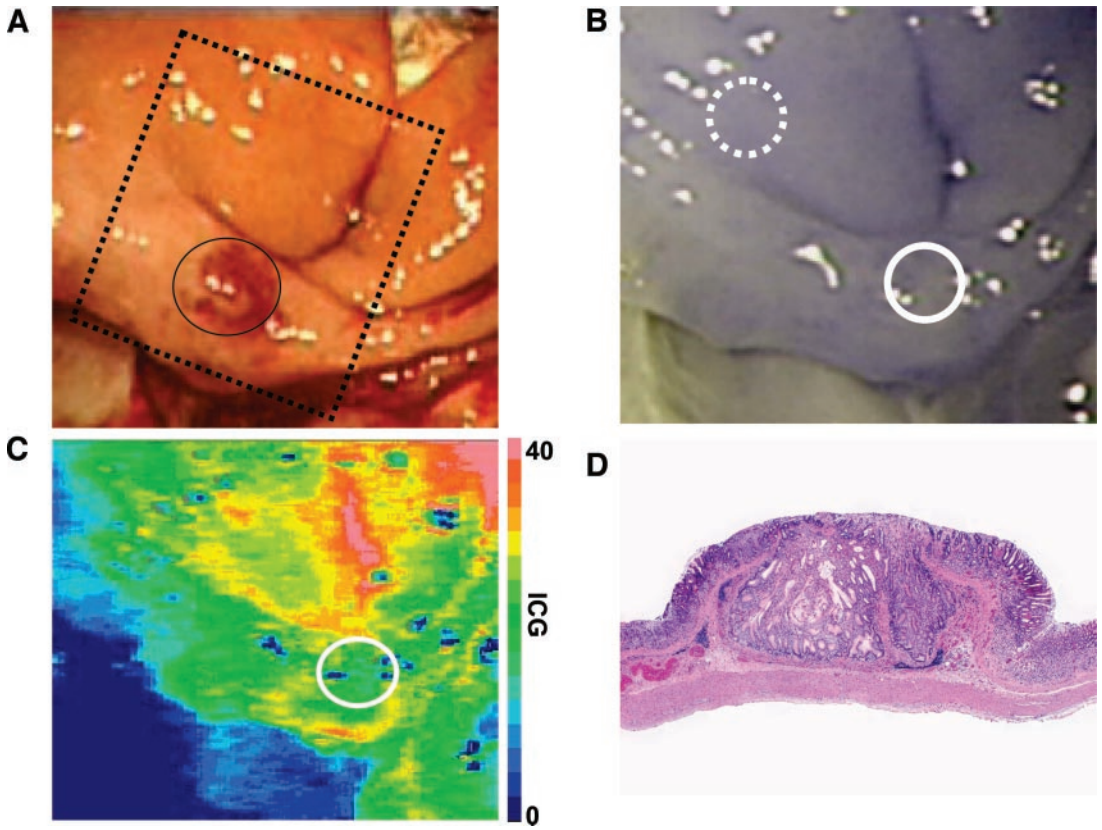

Fig. 7. NIR images of ICG uptake in the stomach of a gastric tumor-containing rat after bolus intravenous injection of ICG. *A*, a photo of externalized, uplifted, and opened stomach of a living rat. *B*, NIR image of ICG uptake of the gastric mucosa surface of the living rat with cancers. ICG uptake, that is, the arterial blood flow, was shown by the distribution of the dye. There was no difference in the rate of ICG uptake between regions of tumor (*white solid circle*) and normal tissues (*white dashed circle*), except for halation. *C*, pseudo-color map of the distribution of NIR of ICG uptake. There was no significant difference between the tumor (*white solid circle*) and normal tissue (*dashed circle*). *D*, the histology of gastric cancer.

perfusion between tumor and normal tissue in the injured stomach. The histology of the ICG-treated stomach of Fig. 7 is shown in Fig. 7*D* and proves that adenocarcinoma was present and highly differentiated, containing severe necrosis similar to the examples used for the EPRI experiments. Therefore, we concluded that there are no significant differences in either the perfusion or compound distribution rates between normal and tumor regions of the stomach.

DISCUSSION

Studies were performed to determine whether EPR spectroscopy and EPRI techniques could be used to differentiate gastric carcinoma from surrounding normal tissue based on differences in redox metabolism. We observed that after whole body loading with a nitroxide redox label, gastric tumors are clearly distinguishable from normal surrounding tissue. These tumors were observed to be largely devoid of signal and appear as holes in the three-dimensional image data obtained from the stomach. With localized EPR spectroscopy, it was confirmed that these tumors have a relative absence of signal compared with normal surrounding tissue. Therefore, this relative absence of nitroxide signal could reflect either a much more reduced state within the tumor or decreased delivery and uptake of the label by the tumor. In an effort to dissociate the effect of vascular delivery of the label, experiments were performed with direct topical delivery of the label to the mucosal surface of the rapidly excised stomach, and it was observed that even with direct application of nitroxide, a very rapid decay of signal occurred at the location of tumor. Thus, these results indicate that gastric tumors possess a much more reduced state than the surrounding normal tissue with a rapid bioreduction of the nitroxide redox label.

It is believed that the administered nitroxide radicals are readily reduced through the complex system of tissue-reducing enzymes and couples to hydroxylamines that are EPR silent (36). As for the reaction between pro-oxidants such as superoxide and the applied nitroxide radicals, whereas electron transfer to the nitroxide could also occur, the lifetime of these oxidants is very short, and the rate of this reaction is relatively slow, so this pathway is not considered a major contributor to the overall process of reduction in the tissue (37). However, the more rapid reduction of the probe could also reflect a higher flux of electrons through both reducing and pro-oxidant producing pathways.

The EPR image data indicated that the 3-CP nitroxide label was absent from the gastric tumors, although it was otherwise homogeneously distributed over the gastric wall after intravenous administration to the rat. Consistent with this result, pharmacokinetic studies using localized EPR spectroscopy suggested that the lifetime of 3-CP in the tumors was too short to be detected compared with that in the normal stomach tissue, so that only 3-CP remaining in the normal stomach tissue was detected after the 2-minute infusion of 3-CP. We have observed previously that the half-life of 3-CP in normal leg muscle is 14.6 $\pm$ 0.5 minutes (21). In this study, a somewhat shorter value of 8.7 $\pm$ 0.9 minutes was observed from the normal stomach. In view of reports that the concentrations of antioxidants are high in the stomach, with levels above those of other tissues (38), it is expected that the half-life of 3-CP in the normal stomach tissue would be shorter than that in normal skeletal muscle.

Assuming that the lifetime of the nitroxide is determined *in vivo* by the metabolism and distribution of nitroxide (17, 39), the short lifetime of 3-CP in the cancer tumors could be explained by a combination of the following three factors: (*a*) lower delivery of 3-CP by the circulation, (*b*) increased metabolic conversion of the nitroxide to the EPR-inactive form by the endogenous reducing agents, and (*c*) enhancement of bioreduction in the tumor under hypoxic conditions. It has been reported that the levels of endogeneous reducing agents such as thiols and ascorbic acid, which can rapidly reduce the nitroxide, are increased in gastric cancer (40, 41). It has also been reported that the blood flow of tumors such as carcinosarcoma can be lower than that in the normal stomach (42). When the infusion rate is low in the endogenous reducing agent-rich tissue, the amount of delivered nitroxide and its contact time with the endogenous reducing agent would be increased, resulting in an increase in the amount of the reduced nitroxide. In addition, many tumors contain a high hypoxic fraction, in which bioreduction is enhanced (26, 27, 39). In prior EPRI studies of implanted fibrosarcoma, it was reported that 3-fold lower pO_2 values are present within the tumor and are accompanied by much more rapid nitroxide reduction in the tumor compared with that in normal tissue (21). The reduced state of tumors could also be due to intermittent hypoxia (43, 44). In our model, NIR imaging of tissue perfusion demonstrated that there was no significant difference in perfusion of the tumor and the normal tissue, which suggests that the rapid 3-CP clearance observed was due primarily to metabolic reduction.

Alterations in oxygen radical generation and tissue redox state are key factors in the process of carcinogenesis (45). There is evidence that enhanced oxidant stress is a key factor in tumor promotion and oncogenesis (46). With regard to gastric carcinoma, it has been shown in the model we used that MNNG treatment induces increased oxygen radical generation, and this is thought to be an important process in triggering cellular transformation leading to tumor formation (7). It is also clear from the literature that marked increases in oxygen radical generation as triggered by radiation treatment or certain types of chemotherapy including anthracyclines are effective in inducing tumor cell death (11, 12).

There have been a number of studies reporting that after oxidant stress, there is an increased reduction of nitroxides in biological tissues (25, 47). This phenomenon has been reported in a number of tissues including the lungs, brain, and heart. It is possible that after oxidant stress, there is a cellular compensatory response resulting in induction of antioxidative enzymes and increased levels of antioxidants. It is possible in tumors that such an antioxidant response with a higher reduced state could render resistance to radiation or other therapies. In addition to enhanced levels of antioxidants or antioxidative enzymes, it is possible that pro-oxidant enzyme pathways could be suppressed. Indeed, it has been reported previously that a number of human tumors are associated with an absence of p53, and we have observed previously that p53-induced genes are involved in oxidant formation leading to cellular apoptosis (10). Thus, one can hypothesize that after a prolonged sublethal oxidant exposure, there could be altered gene expression with transformation of the cellular phenotype to a highly reduced antioxidative state. This, in turn, would tend to protect the cell from regulatory pathways that would otherwise lead to apoptotic cell death. Thus, the ability to assess the cellular redox state of transformed cells and tumors could be of particular importance in identifying the cellular phenotype and optimizing therapeutic approaches for tumor cell killing.

Whereas EPRI measures free radical metabolism and overall redox state, it is not specific for the cause of alterations in redox state. With inflammatory reactions without limited oxygen supply, the redox state would be expected to shift to a more oxidized condition, and one would expect the rate of nitroxide reduction to be slowed. Prior *in vivo* and *ex vivo* examples in the literature of this have been reported, including the effect of ultraviolet light on the skin of human volunteers or in the postischemic rat heart (17, 48). In the current study, EPRI was applied to measure the redox state of tumor *versus* normal tissue by measuring the reduction rate of administered nitroxide free radicals. By comparing the reduction rate in different spatial locations, the tissue redox state can be differentiated. In the case of mucosal injury and inflammation, the redox state may be different from that in the tumor area, so that EPRI can potentially be used to differentiate the tumor tissue *versus* the injured and inflamed mucosa. However, in our imaging study, there was no apparent inflammatory infiltration in the tumor area of the stomach shown from the histologic slices.

The detection of the redox state of tumors by EPRI could be particularly useful with regard to the choice and optimization of cancer chemotherapy or radiation treatment regiments as well as in the assessment of the efficacy of this treatment. Recent clinical studies (28) have demonstrated unequivocally that the extreme reduced state in solid tumors causes resistance to some anticancer drugs (49–51) and causes the extracellular pH to decrease (52), which also renders some drugs ineffective (53, 54). However, other drugs remain effective in killing hypoxic cancer cells. Low oxygenation has also been reported to accelerate malignant progression and metastasis (29, 55). The ability of EPR methods to not only measure redox state but also provide measurement and spatial mapping of tissue oxygenation should also be very useful in this regard. Thus, EPR spectroscopy and imaging techniques could be of particular use in selection and monitoring of cancer treatment.

As such, the ability to noninvasively and nondestructively identify and image tumor tissue based on its altered redox state and oxygenation should be of particular value both in defining the basic mechanisms of oncogenesis and in optimizing therapies to treat cancer. The application of EPRI reported here is an early attempt to assess the ability of this recently developed technique to provide this type of critical information. Whereas the results obtained here are encouraging in that, in the gastric cancer model studies, the tumor could be visualized, and its redox state could be differentiated from that of the surrounding normal tissue, there are a number of further advances and developments that will be required to realize the full potential of this technique and to advance its eventual use in the important areas of cancer diagnosis and treatment. The major advances required include the development and testing of suitable clinically applicable redox or oximetry paramagnetic probes, as well as further instrumentation advances enabling higher sensitivity detection on larger samples.

At present, applications of *in vivo* EPRI have been restricted mostly to studies in small animals. These limitations have been based on the magnet geometries used, as well as limitations of the radiofrequency that can penetrate larger biological objects and related sensitivity concerns. Recently, we have performed the first applications of this technology to humans with the performance of topical EPR measurements and imaging of nitroxides in normal human volunteers (17). These studies have successfully provided measurement and imaging of the tissue redox state in small, defined regions close to the surface. To date, EPRI has been used for imaging studies of human volunteers by several groups (17, 18, 56, 57). Future clinical applications may be facilitated by localized EPR spectroscopy and imaging with surface resonators or implantable resonators. This approach can optimize local sensitivity and limit the amount of required EPR probe, facilitating applications. The unique ability of EPR spectroscopy and imaging to measure tissue oxygenation and redox state has been proposed to be particularly useful in peripheral vascular disease, radiation and other tumor treatment, and tumor diagnosis, with related efforts under investigation in several groups to advance this technique from the basic research laboratory to clinical application.

In conclusion, our results demonstrate redox differences between normal and tumor cells *in vivo*. Based on this, we observe that EPR spectroscopy and imaging techniques enable identification and visualization of gastric carcinoma in the stomach of rats. These tumors possess a highly reduced state. The ability of this methodology to provide spatial mapping of tissue redox state as well as tissue oxygenation should be particularly useful in studies assessing the role of oxidant-mediated induction of cancer and the efficacy of anticancer therapies. With further technical and pharmacological advances, in the future this methodology could potentially provide valuable information regarding the clinical diagnosis and treatment of cancer.

ACKNOWLEDGMENTS

We thank Dr. Shingo Ishiguro for his help in the histological pictures.

REFERENCES

1. Trends in deaths and death rates. In: Statistics and Information Department, Vital Statistics of Japan 1999. Tokyo, Japan: Health and Welfare Statistics Association; 2001. p. 176.
2. Pisani P, Parkin DM, Bray F, Ferlay J. Estimates of the worldwide mortality from 25 cancers in 1990. Int J Cancer 1999;83:18–29.
3. Richardson HL. Induction of adenocarcinoma of the glandular stomach in rats by alcohol gastric lavage and feeding acetylaminofluorene. Proc Am Assoc Cancer Res 1961;2:141–2.
4. Stewart HL, Snell KC, Hare WV. Histopathogenesis of carcinoma induced in the glandular stomach of C 57 BL mice by the intranural injection of 20-methylcholanthrene. J Natl Cancer Inst (Bethesda) 1958;83:999–1019.
5. Stewart HL, Snell KC, Morris HP, Wagner BP, Ray FE. Carcinoma of the glandular stomach of rats ingesting N-N′-2,7-fluorenylenebisacetamide. J Natl Cancer Inst Monogr 1961;5:105–9.
6. Sugimura T, Fujimura S. Tumor production in glandular stomach of rat by N-methl-N′-nitro-N-nitrosoguanidine. Nature (Lond) 1967;216:943–4.
7. Mikuni T, Tatsuta M, Kamachi M. Production of hydroxyl-free radical by reaction of hydrogen peroxide with N-methyl-N′-nitro-N-nitrsoguanidine. Cancer Res 1985;45:6442–5.
8. Tatsuta M, Mikuni T, Taniguch H. Protective effect of butylated hydroxytoluene against induction of gastric cancer by N-methyl-N′-nitro-N-nitrosoguanidine in Wistar rats. Int J Cancer 1983;32:253–4.
9. Irani K, Xia Y, Zweier JL, et al. Mitogenic signaling mediated by oxidants in Ras-transformed fibroblasts. Science (Wash DC) 1997;275:1649–52.
10. Polyak K, Xia Y, Zweier JL, Kinzler KW, Vogelstein B. A model for p53-induced apoptosis. Nature (Lond) 1997;389:300–5.
11. Zweier JL. Reduction of O_2 by iron-Adriamycin. J Biol Chem 1984;259:6056–8.
12. Gianni L, Zweier JL, Levy A, Myers CE. Characterization of the cycle of iron-mediated electron transfer from Adriamycin to molecular oxygen. J Biol Chem 1985;260:6820–6.
13. Berliner LJ, Fujii H, Wan XM, Lukiewicz SJ. Feasibility study of imaging a living murine tumor by electron paramagnetic resonance. Magn Reson Med 1987;4:380–4.
14. Kazama S, Takashige G, Yoshioka H, et al. Dynamic electron spin resonance (ESR) imaging of the distribution of spin labeled dextran in a mouse. Magn Reson Med 1996;36:547–50.
15. Kuppusamy P, Chzhan M, Vij K, et al. Three-dimensional spectral-spatial EPR imaging of free radicals in the heart: a technique for imaging tissue metabolism and oxygenation. Proc Natl Acad Sci USA 1994;91:3388–92.
16. Zweier JL, Chzhan M, Samouilov A, Kuppusamy P. Electron paramagnetic resonance imaging of the rat heart. Phys Med Biol 1998;43:1823–35.
17. He G, Samouilov A, Kuppusamy P, Zweier JL. In vivo EPR imaging of the distribution and metabolism of nitroxide radicals in human skin. J Magn Reson 2001;148:155–64.
18. Rossi S, Giuntini A, Balzi M, Becciolini A, Martini G. Nitroxides and malignant human tissues: electron spin resonance in colorectal neoplastic and healthy tissues. Biochim Biophys Acta 1999;1472:1–12.
19. Chzhan M, Kuppusamy P, Zweier JL. Development of an electronically tunable L-band resonator for EPR spectroscopy and imaging of biological samples. J Magn Reson B 1995;108:67–72.
20. Zweier JL, Kuppusamy P. Electron paramagnetic resonance measurements of free radicals in the intact beating heart: a technique for detection and characterization of free radicals in whole biological tissues. Proc Natl Acad Sci USA 1988;85:5703–7.
21. Kuppusamy P, Afeworki M, Shankar RA, et al. In vivo electron paramagnetic resonance imaging of tumor heterogeneity and oxygenation in a murine model. Cancer Res 1998;58:1562–8.
22. Kuppusamy P, Ohnishi ST, Numagami Y, Ohnishi T, Zweier JL. Three-dimensional imaging of nitric oxide production in the rat brain subjected to ischemia-hypoxia. J Cereb Blood Flow Metab 1995;15:899–903.
23. Kuppusamy P, Chzhan M, Wang P, Zweier JL. Three-dimensional gated EPR imaging of the beating heart: time-resolved measurements of free radical distribution during the cardiac contractile cycle. Magn Reson Med 1996;35:323–8.
24. Chen K, Glockner JF, Morse PD, II, Swartz HM. Effects of oxygen on the metabolism of nitroxide spin labels in cells. Biochemistry 1989;28:2496–501.
25. Utsumi H, Ichikawa K, Takeshita K. In vivo ESR measurements of free radical reactions in living mice. Toxicol Lett 1995;82–83:561–5.
26. Quaresima V, Ursini CL, Gualtieri G, Sotgiu A, Ferrari M. Oxygen-dependent reduction of a nitroxide free radical by electron paramagnetic resonance monitoring of circulating rat blood. Biochim Biophys Acta 1993;1182:115–8.
27. Thomlinson RH, Gray LH. The histological structure of some human lung cancers and the possible implications for radiotherapy. Br J Cancer 1955;9:539–49.
28. Brown JM. The hypoxic cell: a target for selective cancer therapy-eighteenth Bruce F. Cain Memorial Award lecture. Cancer Res 1999;59:5863–70.
29. Hockel M, Schlenger K, Aral B, et al. Association between tumor hypoxia and malignant progression in advanced cancer of the uterine cervix. Cancer Res 1996;56:4509–15.
30. Tatsuta M, Itoh T, Okuda S, Taniguchi H, Tamura H. Effect of prolonged administration of gastrin on experimental carcinogenesis in rat stomach induced by N-methyl-N′-nitro-N-nitrosoguanidine. Cancer Res 1977;37:1808–10.
31. Kuppusamy P, Wang P, Zweier JL, et al. Electron paramagnetic resonance imaging of rat heart with nitroxide and polynitroxyl-albumin. Biochemistry 1996;35:7051–7.
32. Kuppusamy P, Chzhan M, Zweier JL. Development and optimization of three-dimensional spatial EPR imaging for biological organs and tissues. J Magn Reson B 1995;106:122–30.
33. Gurfinkel M, Thompson AB, Ralston W, et al. Pharmacokinetics of ICG and HPPH-car for the detection of normal and tumor tissue using fluorescence, near-infrared reflectance imaging: a case study. Photochem Photobiol 2000;72:94–102.
34. Tatsuta M, Iishi H, Yamamura H, et al. Effect of cimetidine on inhibition by tetragastrin of carcinogenesis induced by N-methyl-N′-nitro-N-nitrosoguanidine in Wistar rats. Cancer Res 1988;48:1591–5.
35. He G, Evalappan SP, Hirata H, et al. Mapping of the B1 field distribution of a surface coil resonator using EPR imaging. Magn Reson Med 2002;48:1057–62.
36. Blackburn RV, Spitz DR, Liu X, et al. Metabolic oxidative stress activates signal transduction and gene expression during glucose deprivation in human tumor cells. Free Radic Biol Med 1999;26:419–30.
37. Samuni A, Krishna CM, Mitchell JB, Collins CR, Russo A. Superoxide reaction with nitroxides. Free Radic Res Commun 1990;9:241–9.
38. Boyd SC, Sasame HA, Body MR. High concentrations of glutathione in glandular stomach: possible implications for carcinogenesis. Science (Wash DC) 1979;205:1010–2.
39. Hahn SM, Sullivan FJ, DeLuca AM, et al. Evaluation of tempol radioprotection in a murine tumor model. Free Radic Biol Med 1997;22:1211–6.
40. Eapen CE, Madesh M, Balasubramanian KA, et al. Mucosal mitochondrial function and antioxidant defenses in patients with gastric carcinoma. Scand J Gastroenterol 1998;33:975–81.
41. Agus DB, Vera JC, Golde DW. Stromal cell oxidation: a mechanism by which tumors obtain vitamin C. Cancer Res 1999;59:4555–8.
42. Sakaeda T, Fukumura K, Takahashi K, et al. Blood flow rate in normal and tumor-bearing rats in conscious state, under urethane anesthesia, and during systemic hypothermia. J Drug Target 1998;6:261–72.
43. Dewhirst MW. Concepts of oxygen transport at the microcirculatory level. Semin Radiat Oncol 1998;8:143–50.
44. Chaplin DJ, Olive PL, Durand RE. Intermittent blood flow in a murine tumor: radiobiological effects. Cancer Res 1987;47:597–601.
45. Takabe W, Niki E, Uchida K, et al. Oxidative stress promotes the development of transformation:involvement of a potent mutagenic lipid peroxidation product, acrolein. Carcinogenesis (Lond) 2001;22:935–41.
46. Cerutti PA. Prooxidant states and tumor promotion. Science (Wash DC) 1985;227:375–81.
47. Vallyathan V, Leonard S, Kuppusamy P, et al. Oxidative stress in silicosis: evidence for the enhanced clearance of free radicals from whole lungs. Mol Cell Biochem 1997;168:125–32.
48. Velayutham M, Li H, Kuppusamy P, Zweier JL. Mapping ischemic risk region and necrosis in the isolated heart using EPR imaging. Magn Reson Med 2003;49:1181–7.
49. Rice GC, Hoy C, Schimke RT. Transient hypoxia enhances the frequency of dihydrofolate reductase gene amplification in Chinese hamster ovary cells. Proc Natl Acad Sci USA 1986;83:5978–82.
50. Shen J, Hughes C, Chao C, et al. Coinduction of glucose-regulated proteins and doxorubicin resistance in Chinese hamster cells. Proc Natl Acad Sci USA 1987;84:3278–82.
51. Hughes CS, Shen JW, Subjeck JR. Resistance to etoposide induced by three glucose-regulated stresses in Chinese hamster ovary cells. Cancer Res 1989;49:4452–4.
52. Skovsgaard T. Transport and binding of daunorubicin, Adriamycin, and rubidazone in Ehrlich ascites tumor cells. Biochem Pharmacol 1977;26:215–22.
53. Tannock I, Guttman P. Response of Chinese hamster ovary cells to anticancer drugs under aerobic and hypoxic conditions. Br J Cancer 1981;43:245–8.
54. Teicher BA, Holden SA, al-Achi A, Herman TS. Classification of antineoplastic treatments by their differential toxicity toward putative oxygenated and hypoxic tumor subpopulations in vivo in the FSaIIC murine fibrosarcoma. Cancer Res 1990;50:3339–44.
55. Shweiki D, Itin A, Soffer D, Keshet E. Vascular endothelial growth factor induced by hypoxia may mediate hypoxia-initiated angiogenesis. Nature (Lond) 1992;359:843–5.
56. Swartz HM, Walczak T. Developing in vivo EPR oximetry for clinical use. Adv Exp Med Biol 1998;454:243–52.
57. Miyake M, Liu KJ, Walczak TM, Swartz HM. In vivo EPR dosimetry of accidental exposures to radiation: experimental results indicating the feasibility of practical use in human subjects. Appl Radiat Isot 2000;52:1031–8.

In vivo Detection of Gastric Cancer in Rats by Electron Paramagnetic Resonance Imaging

Tomiko Mikuni, Guanglong He, Sergey Petryakov, et al.

Cancer Res 2004;64:6495-6502.